Crossed Beam Photodissociation Imaging of HeH^+ with Vacuum Ultraviolet Free-Electron Laser Pulses

H. B. Pedersen,[1,*] S. Altevogt,[1] B. Jordon-Thaden,[1] O. Heber,[2] M. L. Rappaport,[2] D. Schwalm,[1] J. Ullrich,[1] D. Zajfman,[1,2] R. Treusch,[3] N. Guerassimova,[3] M. Martins,[4] J.-T. Hoeft,[4] M. Wellhöfer,[4] and A. Wolf[1]

[1]*Max-Planck-Institut für Kernphysik, D-69117 Heidelberg, Germany*
[2]*Department of Particle Physics, Weizmann Institute of Science, Rehovot, 76100, Israel*
[3]*HASYLAB, DESY, Hamburg, Germany*
[4]*Institut für Experimentalphysik, Universität Hamburg, D-22761 Hamburg, Germany*

(Received 21 February 2007; published 1 June 2007)

Molecular photofragmentation has been studied by event imaging on HeH^+ ions at 32 nm (38.7 eV) in a fast ion beam crossed with the free-electron laser in Hamburg (FLASH), analyzing neutral He product directions and energies. Fragmentation into $He(1snl, n \geq 2) + H^+$ was observed to yield significant photodissociation at 32 nm with an absolute cross section of $(1.4 \pm 0.7) \times 10^{-18}$ cm^2, releasing energies of 10–20 eV. A clear dominance of photodissociation perpendicular to the laser polarization was found in contrast to the excitation paths so far emphasized in theoretical studies.

DOI: 10.1103/PhysRevLett.98.223202 PACS numbers: 34.80.Gs

With the advent of the intense, pulsed free-electron laser in Hamburg (FLASH) at DESY, Germany [1], photofragment imaging of molecular ions and radicals has become feasible for vacuum-ultraviolet (VUV) and soft x-ray wavelengths below 100 nm using dilute fast moving ion targets in the crossed-beams geometry. In this method the momenta of fragments emerging after photoabsorption are directly measurable with space and time resolving particle detectors using three-dimensional event-by-event reaction imaging for all charged as well as neutral products. Hence, chemical dynamics on the high-lying potential surfaces reached by energetic photons can now be probed for a wide range of species and fragmentation channels inaccessible so far, extending from elementary ionic molecules up to larger systems with numerous neutral fragments even after multiple ionization by x-ray photons.

Here we report results from a first path-finding crossed-beams imaging experiment on the photodissociation of HeH^+ at 32 nm, detecting events leading to neutral He fragments and analyzing the kinetic energy release and the angular orientation of the dissociating molecule with respect to the photon polarization. The experiment uses a pulsed mass-selected monoenergetic ion beam at several kilo-electron-volt laboratory energy and an ion-photon interaction zone kept under ultrahigh vacuum. From the energy releases measured with three-dimensional reaction imaging we find significant contributions of highly excited product states $He(1snl)$ with $n \geq 3$ and the angular analysis reflects excited molecular states with symmetries so far not considered as pathways for photodissociation. In addition, we determine the absolute cross section.

HeH^+ is a fundamental benchmark as the simplest heteronuclear ion isoelectronic to H_2 and well understood [2] in the $X^1\Sigma^+$ ground state both theoretically [3,4] and experimentally [5]. Electronically excited states of HeH^+ (Fig. 1) are reached only by high energy input ($\geq$20 eV) and have been addressed theoretically [6–10], including their photodissociation [8–10], and experimentally in electron-impact [11,12] and charge-exchange [13] collision studies; however, their photonic excitation is experimentally largely unexplored. This similarly holds for most small cations since they are only accessible at very low target densities and their study therefore requires an intense source of energetic photons that was so far not available. Beyond the fundamental interest, HeH^+ also attracts attention as the isotopologue of $^3HeT^+$ which is formed in the beta decay of T_2; its excited state properties determine the size of molecular contributions [6,14] to the beta electron energy spectrum addressed with utmost pre-

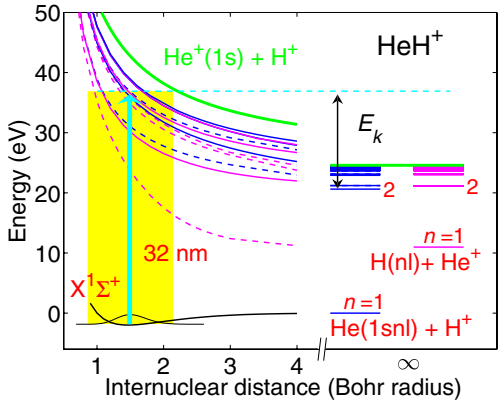

FIG. 1 (color online). Excited potential energy curves, atomic final-state limits, and sample kinetic energy release E_k for HeH^+ photodissociation at 32 nm. The lowest vibrational wave function and the Franck-Condon region for high vibrational excitation are shown schematically for the $X^1\Sigma^+$ ground potential [3] with excited $^1\Sigma^+$ [14] (dashed lines) and $^1\Pi$ states [7] (full lines), the gray scale (colors) indicating the (adiabatic) correlation to the final levels. The upper thick gray lines (green) traces the $He^+ + H^+$ Coulomb potential.

 © 2007 The American Physical Society

cision in upcoming electron-neutrino mass measurements [15]. In this context, a calculated photodissociation cross section of HeH^+ has been presented [10] suggesting this process as a sensitive probe for the advanced electronic structure calculations required. Moreover, in models of the dust-free early Universe [16,17], HeH^+ acts as molecular coolant and has an influence on thermal properties and collapse phenomena. HeH^+ is also assumed to exist (although not definitively observed [18,19]) in several present-day astrophysical plasmas [20] in the vicinity of strong VUV or x-ray sources, e.g., planetary nebula [21], and its chemistry in such environments has been considered in several models [22–24]. Thus, despite strong interest from various fields, no experimental data on the VUV photodissociation of HeH^+ are available to benchmark theoretical predictions.

Fast crossed-beam photodissociation has been studied early on for H_2^+, mainly focusing on the ionic fragments [25]; later, three-dimensional imaging detectors for neutral fragments were implemented for charge-exchange measurements on molecular ion beams (including HeH^+) [26,27] and in strong field studies on H_2^+ (see, e.g., Ref. [28]). The arrangement used here represents a newly created ion-beam infrastructure around the plane-grating monochromator beam line (PG2) [29] at FLASH. Ions were produced in a hollow-cathode ion source and accelerated to a final energy of 4.2 keV. After mass selection in a dipole magnet, the ions were transported a distance of $\sim$5 m through electric steering and focusing giving an average current of $\sim$1 nA at the interaction region. Before the final 90° bend at $\sim$1.2 m from the interaction zone, ion pulses of $\sim$4.5 μs length with $\sim$20 ns rise time were created by electric chopping synchronized to the free-electron laser (FEL) pulses. After the interaction region the HeH^+ ions, forming a $\sim$1 mm-size beam, were electrostatically bent into a Faraday cup connected to a calibrated charge-sensitive amplifier recording the charge in each ion pulse.

VUV pulses from FLASH at 32 ± 0.5 nm cross the ion beam at right angle as shown in Fig. 2 with the photon polarization directed along the ion beam. The FEL output before the monochromator consisted of trains of short ($\sim$30 fs) pulses of 20–30 μJ energy, separated by 10 μs. With a train repetition rate of 5 Hz, five single FEL pulses per train were matched by ion pulses, giving an effective interaction rate of 25 Hz. The FEL light was transported through the monochromator beam line [29] in the zeroth order with a transmission of 30%–50% trading a bandwidth of $\pm$0.5 nm for high photon flux. In the interaction region $\sim$1 m before the final focus of the PG2 beam line, the photon beam had a size of 1–2 mm. Typically $\sim$25 HeH^+ ions collided with $(1–2) \times 10^{12}$ photons per pulse. The FEL pulses were dumped on a negatively biased (-800 V) Cu structure, from which a signal calibrated relative to the FLASH intensity monitors [30] was recorded giving the absolute photon number per pulse. The spatial profiles of the ion and the FEL beams perpendicular to the crossing plane were recorded by moving a 1 mm wide slit positioned at 45° relative to both beams across the interaction region.

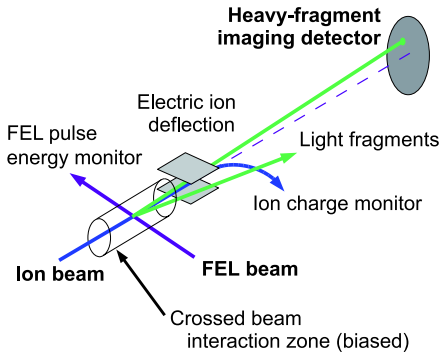

FIG. 2 (color online). Schematic of the crossed-beam imaging setup at the FLASH beam line.

Neutral fragments produced in the FEL-ion crossing and in adjacent ion-beam sections proceeded to a time and position sensitive, 80 mm diam. multi-channel plate (MCP) detector set up perpendicular to the ion-beam axis $\sim$1 m downstream. In addition to the FEL-induced signal, collisional dissociation of the molecular ions in the residual gas ($\sim 5 \times 10^{-10}$ mbar) produced a background of neutrals on this detector. It was significantly reduced by applying a negative bias of 1500–3000 eV over $\sim$3 cm around the crossing point, which locally accelerated the ions in the interaction region. Hence, fragments released from the ion bunch in the biased region reached the MCP detector $\sim$350–600 ns before corresponding fragments created in other sections of the ion path. By timing the FEL pulse to about the middle of the first 500 ns of the ion pulse in the interaction region, the true fragmentation signal was observed at times when only neutrals produced in the short biased region contribute to the background.

Using a delay line anode, the MCP detector yielded counting events representing the transverse position (r_i) of the recorded fragment (i) and its time of flight (t_i) relative to the photon interaction. Stray photons from the FEL were observed promptly after the pulse on the MCP detector, but after centering the FEL beam in the interaction region the photon level was sufficiently low to ensure detection with essentially no photon-induced background during the fragment arrival. The longitudinal velocity in the center-of-mass (c.m.) frame is obtained from the event time t_i as $v_{\parallel i} = (L - v_0 t_i)/t_i$, where $L = 0.987$ m is the detector distance and v_0 the ion-beam velocity in the interaction region; typically, $v_0/L = t_0 = 1.9–2.4$ μs. The transverse fragment velocity is obtained from the distance r_i of the event with respect to the beam center position on the detector as $v_{\perp i} = r_i/t_i$; the kinetic energy release then follows as $E_k = (m_i^2/2\mu)[r_i^2 + (L - v_0 t_i)^2]/t_i^2$, with m_i and μ being the fragment and reduced mass, respectively. For two-body fragmentation the hit positions and times of fragments $i = 1, 2$ are kinematically correlated by energy

and momentum conservation through $r_i^2 = q_i^2(t_i/t_0)^2 - L^2[1-(t_i/t_0)]^2$ with $q_i^2 = L^2(\mu M/m_i^2)E_k/E_0$, using $E_0 = (M/2)v_0^2$, where M is the total mass. In the present experiment, the precise ion energy E_0 was determined from the average time of flight of the photon-induced signal events for runs with $E_0 = 5800$–6700 eV. For the two-dimensional photofragment image in Fig. 3 these runs were added after rescaling them to the nominal value of $\tilde{E}_0 = 7200$ eV keeping $v_\parallel$ and $v_\perp$ constant for each event.

The photofragment image after ~13 h measuring time, Fig. 3(a), in comparison to the background image, Fig. 3(b), taken with the same counting cycle at ~5 μs after each FEL pulse, clearly shows He fragments with large transverse momentum fulfilling the kinematical condition of high (~8–20 eV) kinetic energy release on top of collisional neutralization events characterized by small energy release.

Hydrogen fragments are likely to arise at similar kinetic energy release (see Fig. 1), but are spread out over c.m. velocities and hence event positions larger by a factor of $\sim m_{\mathrm{He}}/m_{\mathrm{H}} = 4$, and the present arrangement only covers ~7% of the solid angle for these fragments. While not discernible in single channels, a weak signal is indeed found in the H kinematical region from the integrated signal versus background counts, consistent with a similar cross section for the $H + He^+$ channel as for $He + H^+$.

The kinetic energy release relates to the initial rovibrational excitation $E(vJ)$ and the final fragment excitation $E(nl)$ as $E_k = E_\gamma + E(vJ) - E(nl) - D_0$, where E_γ is the photon energy, and D_0 is the HeH^+ dissociation energy. The observed kinetic energy distribution for the He fragments after background subtraction is shown in Fig. 4(a). Low E_k corresponds to highly excited states He($1snl$) with a significant fraction of ~50% found in $n \geq 3$. The width of the low-energy edge is consistent with the energy resolution expected for the unmonochromatized photon beam (± 0.6 eV) and the position and time resolution of the detector as presently used (± 0.7 eV, corresponding to ± 0.5 mm and 1 ns bin width for the time). The extension of the high energy edge up to ~21 eV indicates substantial vibrational excitation in the ion source; this will be avoided in later experiments using an electrostatic ion-beam trap integrated in the setup.

The absolute cross section for HeH^+ photodissociation to He($1snl$) + H^+ at 32 nm can be found from the measured ion current I and photon number N_γ of each pulse. Using the transverse beam overlap measurements, the overlap factor representing the integral over the product of the ion and photon density distributions perpendicular to the crossing plane was determined to $F = (3.5 \pm 1.0)$ cm^{-1}. With the number N of observed signal events, the linear ion density $n_l = I/ev_0$ and the channel plate efficiency $\varepsilon = 0.5 \pm 0.1$ the cross section is obtained as $\sigma = N/\varepsilon F \sum N_\gamma n_l$, where $\sum$ denotes the sum over all temporal FEL-ion overlaps. The result is $\sigma = (1.4 \pm 0.7) \times 10^{-18}$ cm^2 where the error of $\pm 50\%$ represents systematic uncertainties from the photon intensity monitoring (about $\pm 20\%$), the detector efficiency, and the overlap factor; the statistical error is $\pm 18\%$.

The fragmentation angle with respect to the photon polarization (along the ion beam) is obtained as $\theta = \arctan[r_i/(L - v_0 t_i)]$, with $\theta = 0$–$180°$ Assuming a fast fragmentation, it represents the molecular orientation at the

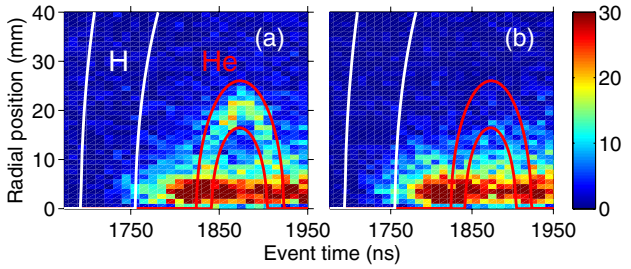

FIG. 3 (color online). Photodissociation image of neutral fragments from HeH^+ at 32 nm measured (a) with $\sim 1.2 \times 10^6$ photon pulses of typically 10 μJ in the crossing region and (b) between photon pulses (background). Counts for given radial position and event time are shown for a nominal ion energy of $\tilde{E}_0 = 7200$ eV after adding several runs as described in the text. Lines indicate constant E_k for He [gray (red) curve] and H (white line) fragments and $E_k = 8$ and 20 eV, respectively.

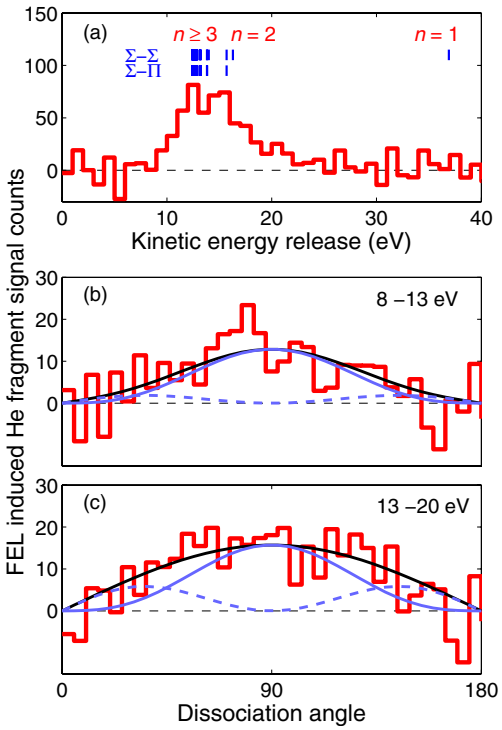

FIG. 4 (color online). Photofragment distributions for HeH^+ at 32 nm. (a) Kinetic energy release (E_k) distribution from imaging of the He fragments, compared with E_k for He($1snl$) final levels. (b),(c) HeH^+ dissociation angle distributions relative to the FEL polarization for $E_k = 8$–13 eV and 13–20 eV, respectively. Full black lines show fitted distributions composed of a dominant $\Sigma - \Pi$ contribution [full gray (blue) curves] plus additional $\Sigma - \Sigma$ contributions (dashed lines).

time of the photoexcitation. Cross sections for transitions from the $X^1\Sigma^+$ ground state to $^1\Sigma^+$ excited states are expected to be strongest for a molecular orientation along the polarization vector ($\theta = 0°$ and 180°, anisotropy parameter $\beta = 2$ [31]), while for $^1\Pi$ excited states they peak at $\theta = 90°$ ($\beta = -1$). The observed angular distributions in Figs. 4(b) and 4(c) show a clear dominance of Σ-Π transitions with fitted contributions of ~90% and ~70%, respectively, for the two ranges of E_k represented.

The observed photodissociation at 32 nm for the final channels $He^+(1s) + H(nl)$ with $n \geq 2$ proceeds via a large manifold of excited HeH^+ potential curves. Only one theoretical study [10] considered the total cross section for a larger subset of such curves, selecting the 12 lowest $^1\Sigma^+$ states correlated to $He^+(1s) + H(nl)$ and $He(1snl) + H^+$, obtaining a local maximum of $\sim 0.8 \times 10^{-18}$ cm^2 near 32 nm in the cross section for the vibrational level $v = 0$. Taking 30% for the observed contribution of this symmetry, the present measurement yields $(0.4 \pm 0.2) \times 10^{-18}$ cm^2 restricted to the $He(1snl) + H^+$ channels and for an unknown vibrational excitation; this reasonably confirms the prediction if the cross sections are assumed to be similar among the various v levels and the two product channels. On the other hand, the lower edge of the fragment energy distribution reveals, for even the $v = 0$ initial levels, an important contribution of higher final excitation ($n \geq 3$) and thus from even higher excited potentials than included by Ref. [10]. Moreover, the major parts of the total cross section arise from excited Π states. A single study [9] considered the contribution of the Π symmetry for the lowest potential curve, showing it to be of similar size as the Σ contribution at 32 nm. The experiment roughly confirms this trend, but clearly shows that higher excitations for both the Π and the Σ symmetries must be included for predictions of the total photodissociation cross section.

Channels beyond the lowest electronic excitation, apart from $n = 1$ product channels, are also not included in the HeH^+ photodissociation rates within available astrophysical models [17,22–24]. In view of the present data, this restriction does not seem to be *a priori* justified, as radiation capable of producing photodissociation through higher excited curves can indeed be available in regions where HeH^+ is formed [23].

These results on the photodissociation of HeH^+ represent a first benchmark for the application of the new intense free-electron laser based light sources in the soft x-ray region on dilute species in fast-particle crossed-beams experiments. Using event-by-event imaging on neutral fragments, the method revealed the kinetic energy release spectrum and molecular orientations during high-energy photon interaction. For HeH^+ this shows the importance of dissociation pathways via states left unconsidered in recent theoretical studies and astrophysical models. Extensions of the system are in progress regarding, among others, the unique definition of the initial vibrational level, better fragment energy resolution, lighter fragments detection (such as H and H^+ from HeH^+), larger target molecules, and coincident detection with both photoelectrons and multiple heavy fragments.

This work has been supported by the Minerva Foundation and the Max-Planck Initiative DESY FEL (MIDFEL). H. B. P. acknowledges support from the European Community program IHP through the Marie Curie Fund under Contract No. HPMF-CT-2002-01833.

*To whom correspondence should be addressed.
Electronic address: henrik.pedersen@mpi-hd.mpg.de

[1] V. Ayvazyan *et al.*, Eur. Phys. J. D **37**, 297 (2006).
[2] J. A. Coxon and P. G. Hajigeorgiou, J. Mol. Spectrosc. **193**, 306 (1999), and references therein.
[3] W. Kolos and J. M. Peek, Chem. Phys. **12**, 381 (1976).
[4] D. M. Bishop and L. M. Cheung, J. Mol. Spectrosc. **75**, 462 (1979).
[5] Z. Liu and P. B. Davis, J. Chem. Phys. **107**, 337 (1997), and references therein.
[6] H. H. Michels, J. Chem. Phys. **44**, 3834 (1966).
[7] T. A. Green *et al.*, J. Chem. Phys. **61**, 5186 (1974); **61**, 5198 (1974); **64**, 3951 (1976).
[8] S. Saha *et al.*, J. Phys. B **11**, 3349 (1978).
[9] D. Basu and A. K. Barua, J. Phys. B **17**, 1537 (1984).
[10] A. Saenz, Phys. Rev. A **67**, 033409 (2003), and references therein.
[11] C. Strömholm *et al.*, Phys. Rev. A **54**, 3086 (1996).
[12] F. B. Yousif and J. B. A. Mitchell, Phys. Rev. A **40**, 4318 (1989).
[13] H. F. Helbig and E. Everhart, Phys. Rev. **136**, A674 (1964).
[14] S. Jonsell *et al.*, Phys. Rev. C **60**, 034601 (1999).
[15] C. Weinheimer, Prog. Part. Nucl. Phys. **57**, 22 (2006).
[16] S. Lepp and J. M. Shull, Astrophys. J. **280**, 465 (1984).
[17] D. Galli and F. Palla, Astron. Astrophys. **335**, 403 (1998).
[18] X.-W. Liu *et al.*, Mon. Not. R. Astron. Soc. **290**, L71 (1997).
[19] S. Miller *et al.*, Nature (London) **355**, 420 (1992).
[20] W. Roberge and A. Dalgarno, Astrophys. J. **255**, 489 (1982).
[21] I. Dabrowski and G. Herzberg, Trans. N.Y. Acad. Sci. **38**, 14 (1977).
[22] J. H. Black, Astrophys. J. **222**, 125 (1978).
[23] D. R. Flower and E. Roueff, Astron. Astrophys. **72**, 361 (1979).
[24] C. Cecchi-Pestellini and A. Dalgarno, Astrophys. J. **413**, 611 (1993).
[25] F. von Busch and G. H. Dunn, Phys. Rev. A **5**, 1726 (1972).
[26] W. J. van der Zande *et al.*, Phys. Rev. Lett. **57**, 1219 (1986).
[27] D. Strasser *et al.*, Phys. Rev. A **61**, 060705 (2000).
[28] I. Ben-Itzhak *et al.*, Phys. Rev. Lett. **95**, 073002 (2005).
[29] M. Martins *et al.*, Rev. Sci. Instrum. **77**, 115108 (2006).
[30] R. Treusch, HASYLAB Annual Report 2005, p. 159.
[31] R. N. Zare, Mol. Photochem. **4**, 1 (1972).